

Modeling Respiratory Mechanics in the MCAT and Spline-Based MCAT Phantoms

W. Paul Segars¹, David S. Lalush^{1,2}, and Benjamin M. W. Tsui^{1,2}

¹Department of Biomedical Engineering and ²Department of Radiology
The University of North Carolina at Chapel Hill, Chapel Hill, NC

Abstract

Respiratory motion can cause artifacts in myocardial SPECT. We incorporate respiratory mechanics into the current 4D MCAT and into the next generation spline-based MCAT phantoms. In order to simulate respiratory motion in the current MCAT phantom, the geometric solids for the diaphragm, heart, ribs, and lungs were altered through manipulation of parameters defining them. Affine transformations were applied to the control points defining the same respiratory structures in the spline-based MCAT phantom to simulate respiratory motion. The NURBS surfaces for the lungs and body outline were constructed in such a way as to be linked to the surrounding ribs. Expansion and contraction of the thoracic cage then coincided with expansion and contraction of the lungs and body. The changes both phantoms underwent were splined over time to create time continuous 4D respiratory models. We conclude that both respiratory models are effective tools for researching effects of respiratory motion.

I. BACKGROUND

Respiratory mechanics involve the motion of the diaphragm, heart, thoracic cage, and lungs [1,2,3]. When the diaphragm contracts, it forces the abdominal contents downward and forward increasing the volume of the thorax. When the diaphragm relaxes, the abdominal contents move upward and inward decreasing the volume of the thorax. The level of the diaphragm can move up and down from 1–10 cm during breathing (Fig. 1). The diaphragm moves about 1 cm during normal tidal breathing [1]. The heart can be seen to move upward and downward in some fashion with the diaphragm. Recent studies suggest that the heart movement is simply a rigid body translation [3]. During respiration, the ribs rotate about an axis through their costal necks to affect the anteroposterior and transverse diameters of the thoracic cavity (Fig. 2). During inspiration, the external intercostal muscle contracts pulling the ribs upward and forward increasing the transverse and anteroposterior diameters of the thorax. During expiration, the internal intercostal muscle contracts pulling the ribs downward and inward decreasing both the transverse and anteroposterior diameters of the thorax. The lungs inflate and deflate with changes in the volume of the thoracic cavity.

Respiratory motion can cause artifacts in myocardial SPECT leading to the misinterpretation of images especially

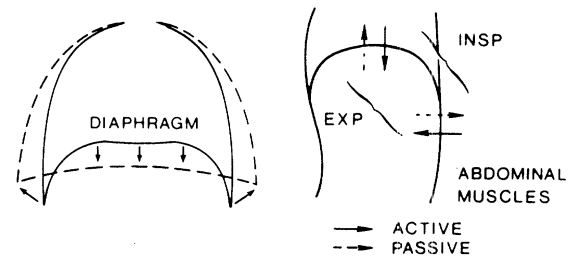


Figure 1: Motion of the diaphragm during respiration [1]. During inspiration, the diaphragm contracts increasing the volume of the thoracic cavity. During expiration, the diaphragm relaxes decreasing the volume of the thoracic cavity.

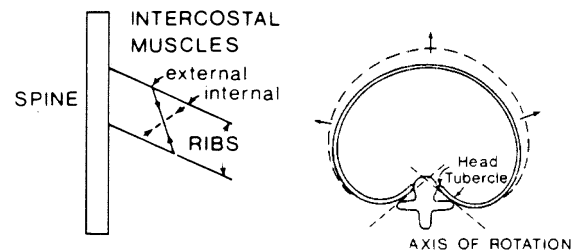


Figure 2: Motion of the ribs during respiration [1]. The ribs rotate about an axis through their costal neck affecting the transverse and anteroposterior diameter of the thoracic cavity.

in the area of the inferior wall of the left ventricle [4]. The artifacts have been shown to be more significant during the expiratory phase due to the attenuation of the inferior uptake by the diaphragm and the scatter from upper abdominal organs such as the liver and stomach [4]. Incorporating respiratory motion into the MCAT phantoms makes them an effective tool to research such effects of respiratory motion.

The 4D Dynamic MCAT phantom [5-8] was developed to permit study of the effects of anatomical variations on cardiac SPECT images [9] and study of gated SPECT [7,10]. Unfortunately, it is limited in its ability to realistically model anatomical variations and patient motion. Thus, a phantom that will model these effects must rely on a different set of primitives to describe the structures in the torso.

An appropriate primitive that will permit the kind of modeling needed is the non-uniform rational B-spline (NURBS) [11,12]. NURBS are widely used in 3D computer graphics to describe three-dimensional surfaces. A NURBS surface (Fig. 3) is a bidirectional parametric representation of an object. Points on a NURBS surface are defined by two parametric variables, u and v , usually representing longitude and latitude respectively.

A 3D NURBS surface of degree p in the u direction and degree q in the v direction is defined as a piecewise ratio of B-spline polynomials by the following function [11,12].

This work was supported by Public Health Service Grant NIH RO1 CA39463. Its contents are solely the responsibility of the authors and do not necessarily represent the official views of the PHS.

$$S(u, v) = \frac{\sum_{i=0}^n \sum_{j=0}^m N_{i,p}(u) N_{j,q}(v) w_{i,j} P_{i,j}}{\sum_{i=0}^n \sum_{j=0}^m N_{i,p}(u) N_{j,q}(v) w_{i,j}} \quad (1)$$

$$0 \leq u \leq 1$$

$$0 \leq v \leq 1$$

The $P_{i,j}$ represent the control points defining the surface, $w_{i,j}$ are weights that determine a point's influence on the shape of the surface, and $N_{i,p}(u)$ and $N_{j,q}(v)$ are the nonrational B-spline basis functions defined on the knot vectors

$$U = \left(\underbrace{0, \dots, 0}_{p+1}, u_{p+1}, \dots, u_{r-p-1}, \underbrace{1, \dots, 1}_{p+1} \right) \quad (2)$$

$$V = \left(\underbrace{0, \dots, 0}_{q+1}, v_{q+1}, \dots, v_{s-q-1}, \underbrace{1, \dots, 1}_{q+1} \right) \quad (3)$$

where $r = n + p + 1$ and $s = m + q + 1$.

NURBS surfaces are continuous; therefore, they permit representation of a surface at any resolution. A disadvantage of NURBS is the mathematical complexities they introduce, but with the increase in complexity comes a vast increase in flexibility to model biological shapes more realistically. Also, NURBS can be altered easily via affine and other transformations to model variations in anatomy among patients. The particular transformation needs only to be applied to the set of control points through a matrix multiplication [13,14].

The spline-based MCAT phantom [13] was developed using the Visible Human Project CT data as a basis to construct 3D NURBS surfaces for torso structures other than the heart. A 4D NURBS model of the beating heart was incorporated from a previous study [14]. The spline-based MCAT phantom can model organ shape and anatomical variations and patient motion more realistically than the current MCAT phantom.

We incorporate respiratory mechanics into the geometry-based MCAT and the spline-based MCAT phantoms. The

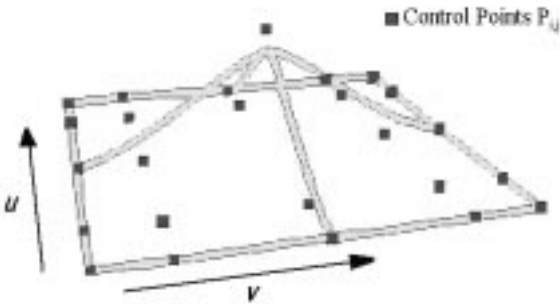


Figure 3: 3D NURBS surface.

resulting NURBS respiratory model is more realistic than the geometry-based model of the MCAT. Both respiratory models, however, can be useful tools in studies involving the effects of respiratory motion.

II. METHODS

The movement of the diaphragm during respiration was simulated in the MCAT phantom by altering the parameter for the height of the left and right diaphragm sections (Top Fig. 4). The movement of the diaphragm in the spline-based MCAT was simulated by translating control points that define the left and right diaphragm surfaces (Bottom Fig. 4). The ratio of the vertical distances between the levels of the control points was kept constant so that the degree of curvature of the diaphragm changed as well as the height. The heart in both phantoms was translated linearly up and down with the movement of the diaphragm.

The ribs in the original MCAT phantom are defined by tilted cut planes through a cylinder (Fig. 5A). This definition does not allow for the ribs to be rotated about the axis through their costal necks. The rotation of the ribs has to be approximated through the parameters that define them. The ribs are defined by three parameters in the current MCAT phantom: the rib long axis, the rib short axis, and the tilt angle of the ribs.

To approximate the change in the transverse diameter of the thoracic cavity due to the rotation of the ribs, the parameter for the long axis of the ribs (RLA) was altered (Fig. 5B). The RLA was simply increased or decreased to change the transverse diameter.

To approximate the change in anteroposterior diameter of the thoracic cavity due to the rib rotation, the parameter for the rib short axis (RSA) was altered (Fig. 5C). Keeping the

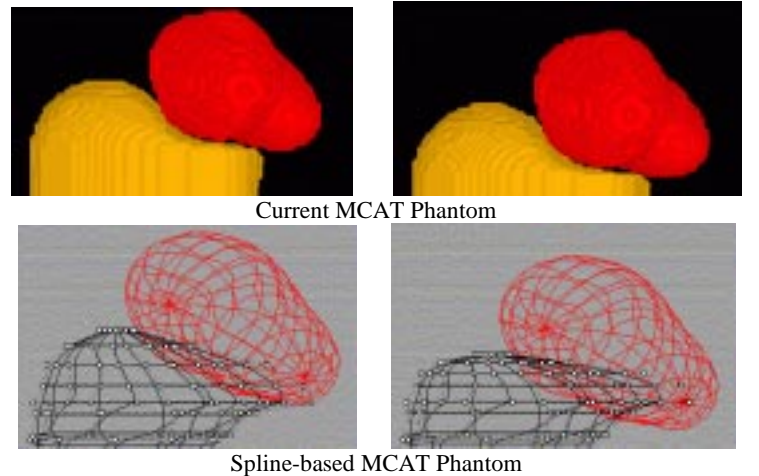


Figure 4: (Top) Parameter for the height of the diaphragm is altered to translate the diaphragm upward and downward in the current MCAT phantom. (Bottom) The control points of the diaphragm in the spline-based MCAT phantom are translated upward and downward to simulate its respiratory movement. The ratio of the vertical distances between the levels of control points is maintained so the degree of curvature changes with the height. The heart moves with the diaphragm in both phantoms. The right portion of the diaphragm is shown in the above examples.

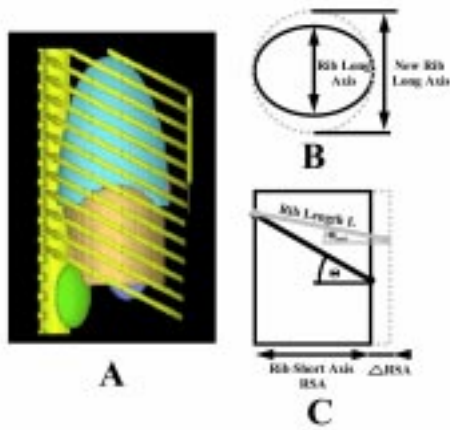


Figure 5: (A) MCAT phantom ribs are defined as tilted cut planes through a cylinder. (B) Transverse diameter change modeled through rib long axis parameter. (C) Anteroposterior diameter change modeled through rib short axis parameter. The tilt angle changes with the change in the rib short axis.

rib length L constant, the tilt angle θ of the cut planes to the horizontal was recalculated according to the amount of change in the rib short axis ΔRSA by equation 4.

$$\theta_{new} = \arccos\left(\frac{RSA + \Delta RSA}{L}\right) \quad (4)$$

The parameters defining the long and short axes of the lung and body were set to increase or decrease with the axes of the ribs.

The spline-based ribs were rotated about the axes of their costal necks (Fig. 2). Control points in each lung were set up to coincide with the ribs (Fig. 6A). The control points were linked to the ribs expanding and contracting the lungs with the rib cage. The cartilage was allowed to stretch with changes in the thoracic cavity. The control points defining the body outline were similarly linked to the ribs (Fig. 6B) allowing the body outline to change with changes in the ribs and lungs.

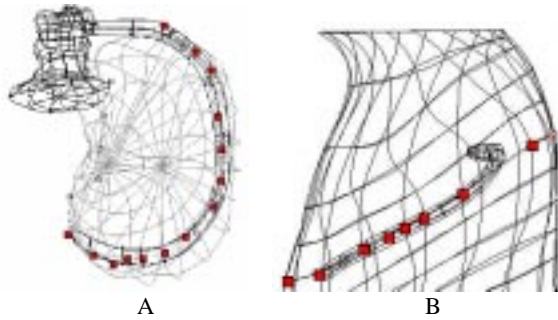


Figure 6: (A) Control points in the left lung coinciding with the rib in the fourth costal arch. (B) Control points in the body outline coinciding with the rib in the fourth costal arch. The closed squares represent control points that move with the rib. The open squares represent unaffected control points.

The sternum in both phantoms was set up to move upward and downward with the movements of the ribs.

The time varying parameters in both phantoms were chosen to fit a volume curve for normal respiration, (Fig. 7A). The period of the respiratory cycle for normal tidal breathing is 5 seconds with inspiration lasting approximately 2 seconds and expiration lasting the remaining 3 seconds. The amount of volume change in the lungs for normal breathing is 500ml. The volume curve was approximated with the piecewise cosine function in equation 5.

$$V(t) = \begin{cases} -250ml \cos\left(\frac{\pi}{2}t\right) + 250 & 0 \leq t \leq 2 \\ -250ml \cos\left(\frac{\pi}{3}(5-t)\right) + 250 & 2 \leq t \leq 5 \end{cases} \quad [5]$$

The top portion of the function represents the volume change during inspiration while the bottom portion represents the volume change during expiration. A graph of the function is shown in figure 7B.

For the current MCAT phantom, the height of the diaphragm and the diameter of the rib short axis were set to change a maximum of 1 cm sinusoidally for normal breathing according to equation 6 and 7 respectively.

$$\Delta_{diaphragm}(t) = \begin{cases} 0.5cm \cos\left(\frac{\pi}{2}t\right) + 0.5 & 0 \leq t \leq 2 \\ 0.5cm \cos\left(\frac{\pi}{3}(5-t)\right) + 0.5 & 2 \leq t \leq 5 \end{cases} \quad [6]$$

$$\Delta_{RSA}(t) = \begin{cases} -0.5cm \cos\left(\frac{\pi}{2}t\right) + 0.5 & 0 \leq t \leq 2 \\ -0.5cm \cos\left(\frac{\pi}{3}(5-t)\right) + 0.5 & 2 \leq t \leq 5 \end{cases} \quad [7]$$

At 17 time frames, the amount of volume change that resulted from altering the two parameters as calculated from equations 6 and 7 was compared to the desired amount of change as calculated from equation 5 to get the volume contribution needed from the long axis parameter. The long axis parameter was set accordingly for the 17 time frames.

For the spline-based phantom, the diaphragm was also set to move 1 cm sinusoidally according to equation 6. The volume change from the diaphragm motion was compared to the volume curve for normal breathing at 17 time frames to get the volume contribution needed from the rotation of the ribs. The amount of rib rotation was set accordingly.

The changes in the parameters for each phantom were

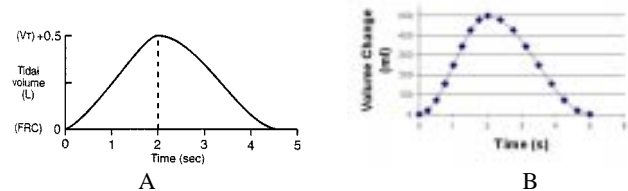


Figure 7: (A) Change in volume curve for normal tidal breathing [1]. (B) Approximation of the volume curve, equation 5.

splined in time creating time continuous 4D respiratory models. The respiratory time curves for the parameters for both phantoms are shown in figure 8. The amplitudes of the time curves for each parameter are adjustable as is the period.

III. RESULTS

Figure 9 displays a coronal cut for the current MCAT and spline-based MCAT phantoms for end-expiration and end-inspiration. Both phantoms illustrate movements similar to that shown in the diagram based on roentgenograms. Figure 10 displays the anterior view of the current MCAT phantom and spline-based MCAT phantom during end-expiration and end-inspiration. Figure 11 shows the right lateral view of both phantoms during end-expiration and end-inspiration. From these images, it is clear that the NURBS surfaces have the potential to model respiratory motion realistically, more so than models based on geometric solids. Thirty time frames were generated from the base seventeen using the motion curves for the parameters. The volume curve for the right lung over the thirty frames for the spline-based MCAT phantom is shown in figure 12. The volume curve for the right lung of the current MCAT phantom is nearly identical to that of the

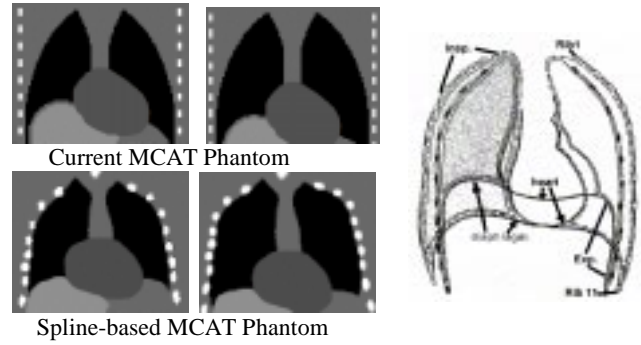


Figure 9: Coronal cut slices of the current MCAT phantom and spline-based MCAT phantom for end-expiration (Left images) and end-inspiration (Middle images). Both phantoms illustrate similar movements to the diagram based on roentgenograms (Right image).

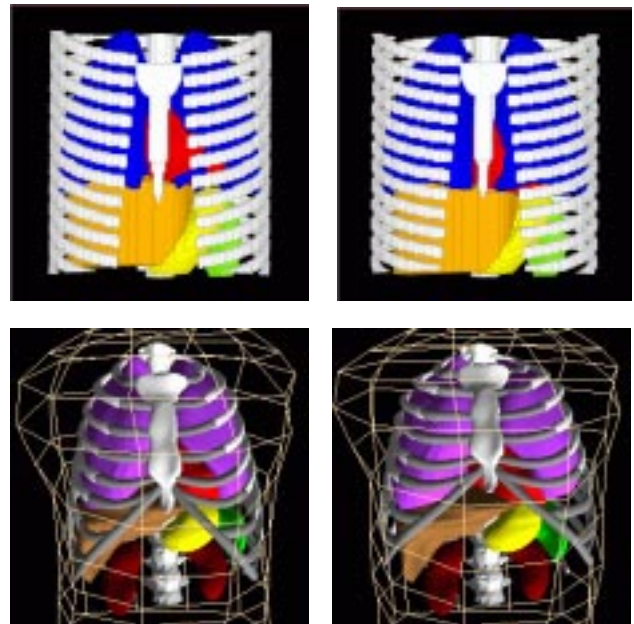
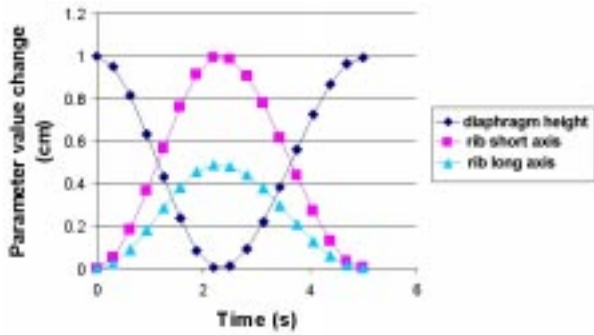
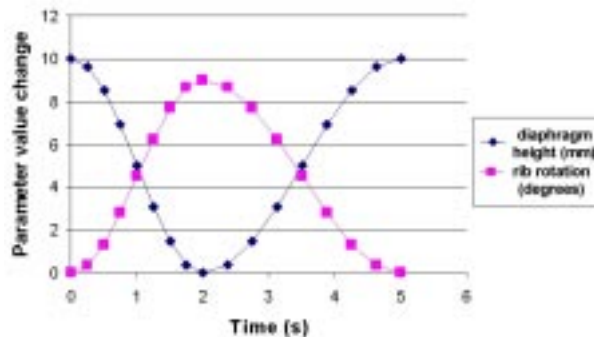


Figure 10: Anterior views of end-expiration (left) and end-inspiration (right) in the current MCAT phantom (Top) and spline-based MCAT phantom (Bottom).



A



B

Figure 8: (A) Parameter curves for the current MCAT phantom over the respiratory cycle. Respiratory parameters for the current MCAT are the diaphragm height, rib short axis, and rib long axis. (B) Parameter curves for the spline-based MCAT phantom over the respiratory cycle. Respiratory parameters for the spline-based MCAT are the diaphragm height and rib rotation.

spline-based phantom. The lung volume change in both models was 500 ml per lung. The thirty frames illustrate a smooth respiratory motion.

IV. CONCLUSIONS

We have developed respiratory models for the current MCAT and the spline-based MCAT phantoms. The spline-based phantom models the respiratory motion more realistically than the geometry-based phantom. Both phantoms, however, offer an important tool in the studies of the effects of respiratory motion.

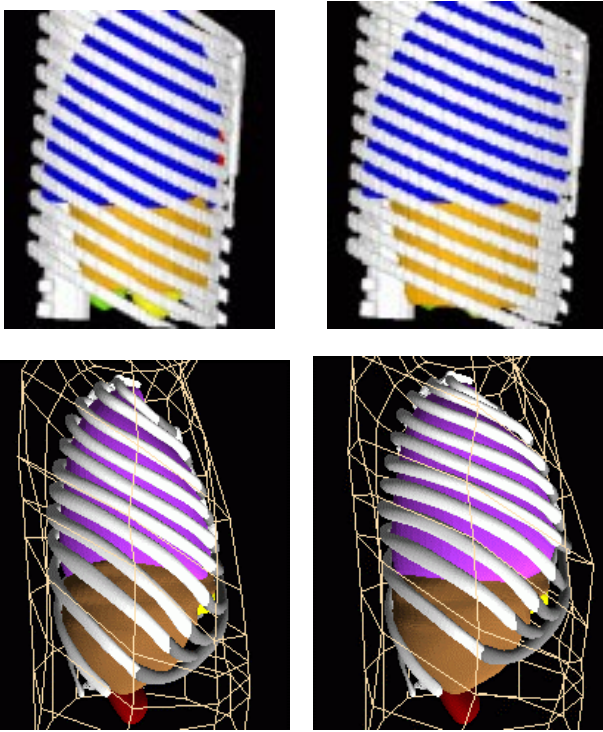


Figure 11: Right lateral views of end-expiration (left) and end-inspiration (right) in the current MCAT phantom (Top) and spline-based MCAT phantom (Bottom).

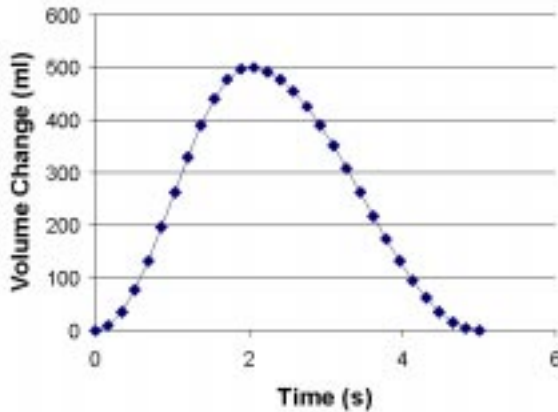


Figure 12: Change in volume curve for the right lung in the spline-based MCAT phantom. The curve for the current MCAT phantom is nearly identical to that of the spine-based phantom.

V. REFERENCES

- [1] J. West, *Respiratory Physiology*, 5th Edition, Williams and Wilkins: Baltimore, 1995.
- [2] W. O. Fenn and H. Rahn, Section 3: Respiration, *Handbook of Physiology*, vol. 1, 1964.
- [3] Y. Wang, S. Riederer, and R. Ehman, "Respiratory motion of the heart: Kinematics and the implications for the spatial resolution in coronary imaging", *MRM*, vol. 33, pp713-719, 1995.
- [4] K. Cho, S. Kumiata, and T. Kumazaki, "Development of respiratory gated myocardial SPECT system," *J Nucl Card*, vol. 6, pp. 20-8, 1999.
- [5] LaCroix KJ, <http://www.bme.unc.edu/mirg/mcat/index.html>.
- [6] Pretorius PH, King MA, Tsui BMW, LaCroix KJ and Xia W. A mathematical model of motion of the heart for use in generating source and attenuation maps for simulating emission imaging. *Med Phys*, 1999, in press.
- [7] B. M. W. Tsui, J. A. Terry, and G. T. Gullberg, "Evaluation of cardiac cone-beam Single Photon Emission Computed Tomography using observer performance experiments and receiver operating characteristic analysis," *Invest Radiol*, vol. 28, pp. 1101-1112, 1993.
- [8] P. H. Pretorius, W. Xia, M. A. King, B. M. W. Tsui, T.-S. Pan, and B. J. Villegas, "Determination of left and right ventricular volume and ejection fraction using a mathematical cardiac torso phantom for gated blood pool SPECT," *J Nucl Med*, vol. 37, pp. 97P, 1996.
- [9] K. J. LaCroix and B. M. W. Tsui, "The effect of defect size, location, and contrast on the diagnosis of myocardial defects in SPECT with and without attenuation compensation," *J Nucl Med*, vol. 37, pp. 20P, 1996.
- [10] D. S. Lalush and B. M. W. Tsui, "Block-iterative techniques for fast 4D reconstruction using *a priori* motion models in gated cardiac SPECT," *Phys Med Biol*, vol. 43, pp. 875-887, 1998.
- [11] L. Piegl, "On NURBS: A Survey," *IEEE Computer Graphics and Applications*, vol. 11, pp. 55-71, 1991.
- [12] L. Piegl and W. Tiller, *The NURBS Book*, 2nd Edition, Springer-Verlag: Berlin, 1997.
- [13] W. P. Segars, D. S. Lalush, and B. W. M. Tsui, "The next generation MCAT: a realistic spline-based torso phantom," *Joint Meeting of BMES and EMBS*, 1999.
- [14] Segars WP, Lalush DS, and Tsui BMW, "A Realistic spline-based dynamic heart phantom," *Trans. On Nsci.*, June 1999.